476958

September 1, 1992

A final report for

HQ GRANT
IN-46-CR
121341
P.62

STUDIES OF INTERACTIVE PLASMA PROCESSES IN THE POLAR CUSP

NASA Grant No.: NAGW-1657

SwRI Project No.: 15-2783

Submitted by:

Dr. J. Hunter Waite, Jr., Principal Investigator
Space Sciences Division
Southwest Research Institute
San Antonio, Texas

SOUTHWEST RESEARCH INSTITUTE
Instrumentation and Space Research Division
6220 Culebra Road, San Antonio, Texas 78238
(512) 684-5111 • FAX (512) 647-4325

A *final report for*

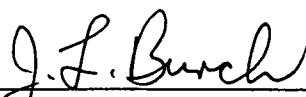## STUDIES OF INTERACTIVE PLASMA PROCESSES IN THE POLAR CUSP

NASA Grant No.: NAGW-1657

SwRI Project No.: 15-2783

Submitted by:

Dr. J. Hunter Waite, Jr., Principal Investigator
Space Sciences Division
Southwest Research Institute
San Antonio, Texas

Approved:

J. F. Burch

Dr. James L. Burch, Vice President
Instrumentation and Space Research Division

This is a final report for NAGW-1657 (SwRI Project 15-2783). Several distinctly different areas of research have been pursued under this grant and are enumerated below.

1.   Studies of the thermal structure of polar outflows:

The emphasis on this portion of the research is the development of an interactive data analysis program for thermal ion analysis of the Dynamics Explorer/ Retarding Mass Spectrometer (DE/RIMS) data. An X-windows code to perform this analysis has recently been completed and is now in the testing phase at NASA/ Marshall Space Flight Center. A copy of the interactive display is included as Appendix A. Future work (under NASA grant NAG5-1554) will now proceed to analyze DE/RIMS ion outflow data. Expected results are the composition, flux, and temperature of terrestrial ion outflows at high latitudes.

2.   Prognoz data analysis:

A recent visit from Dr. Oleg Vaisberg of the Russian Space Institute has provided an opportunity to examine ion and electron particle data at high latitudes over the northern polar cap which were obtained by Dr. Vaisberg's particle experiment aboard the Prognoz-8 spacecraft. A program has been developed for subtracting the sun pulse signal from the data to allow the processing of the low intensity ion flux data in the magnetospheric lobes. From this analysis we hope to gain information about the dayside source region for the observed ion beams and to also use this data as a probe of the dynamic motion of the magnetospheric lobes. The processing of the data using this program will continue under NASA grant NAG5-1554. The data provide a unique opportunity, since no US mission has sampled this high latitude magnetospheric lobe region.

3.   Ulysses Jupiter encounter:

A paper was presented at the annual Division of Planetary Studies of the American Astronomical Society held in Palo Alto in November of 1991 entitled "Jovian Bremsstrahlung X Rays: A Ulysses Prediction" which predicted the Jovian auroral X ray flux that should be measured by the Ulysses Gamma Ray Burst experiment during the Ulysses spacecraft's closest encounter with Jupiter in February of 1992.

The Ulysses' prediction paper generated much interest from people studying the Jovian aurora and from experimenters on the Ulysses spacecraft. As a result of this interest two things happened: 1) a paper of the same title was submitted and accepted for publication in the January issue of the Geophysical Research Letters (see Appendix B), and 2) a massive observing campaign was organized to provide supporting ultraviolet and infrared observations at the time of the Ulysses encounter. This observational interest allowed personnel at SwRI (Alan Stern, PI; Hunter Waite Co-I) to obtain director's discretionary time on the Hubble Space Telescope to support the Ulysses encounter by obtaining ultraviolet observations. A preliminary draft of the paper reporting these results is included as Appendix C.
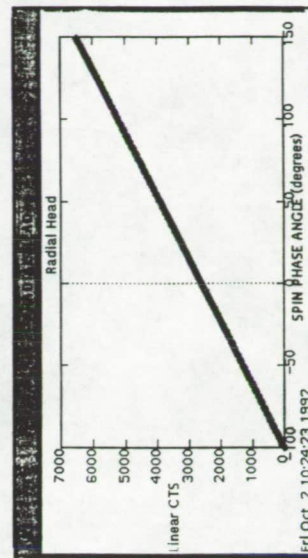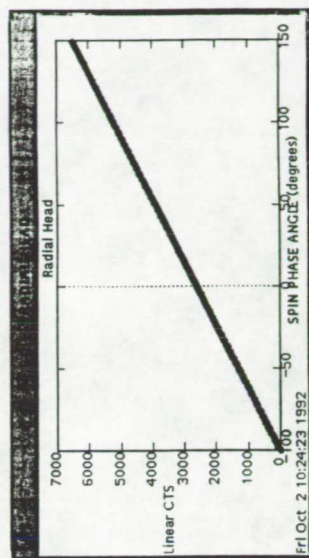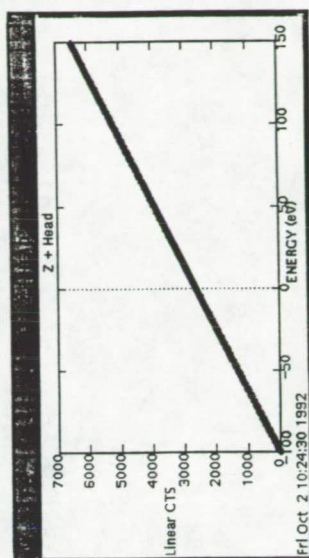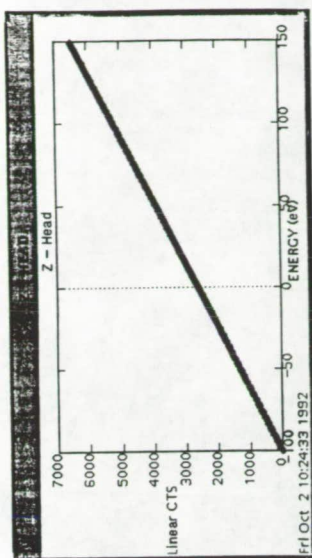
APPENDIX A

H +

R_E = 0.000e+00
LT = 0.000e+00
MLAT = 0.000e+00
L = 0.000e+00
ILAT = 0.000e+00

TIME LIMITS 00/000 00:00:00 - 00:00:00

INCREMENT: 6.00e+01 DURATION: 6.00e+01

START PHASE: −1.80e+02 STOP PHASE: 1.80e+02

START RPA: 0.00e+00 STOP RPA: 1.00e+03

APERTURE BIAS: ☑ ALL

ANGLE BINS:

ION: H+ He+ He++ N+ O+ O++

UPDATE

PLOT LIMITS

Radial:
START PHASE: −1.80e+02 STOP PHASE: 1.80e+02
CTS SCALE LOG LINEAR CTS SCALE

Z HEADS:
START ENERGY: 0.00e+00 STOP ENERGY: 1.00e+03
ENERGY SCALE: LOG LINEAR DATA FILES
CTS SCALE LOG LINEAR CTS SCALE

UPDATE

INITIALIZATION

R/VD DETER n = 5.000e+01 5.000e+01
6.000e+01 7.000e+01 8.000e+01
V_D X: 6.000e+01 Y: 7.000e+01 Z: 8.000e+01
S/C POTENTIAL DETER 4.000e+01 4.000e+01

MODEL
Setting: ☑ O BIMAX

PARAMETERS
n 5.000e+01
$T_{\parallel}$
$T_{\perp}$
V_D X: 6.000e+01 Y: 7.000e+01 Z: 8.000e+01
$P_{s/c}$ 4.000e+01

UPDATE OPTIMIZE

NEXT TIME

REDRAW PRINT

PARAMETERS

n	5.000e+01
$T_{\parallel}$	0.000e+00
$T_{\perp}$	0.000e+00
V_D X:	6.000e+01
Y:	7.000e+01
Z:	8.000e+01
$P_{s/c}$	4.000e+01

Plot 1: Z − Head — Linear CTS vs ENERGY (eV) — Fri Oct 2 10:24:33 1992

Plot 2: Z + Head — Linear CTS vs ENERGY (eV) — Fri Oct 2 10:24:30 1992

Plot 3: Radial Head — Linear CTS vs SPIN PHASE ANGLE (degrees) — Fri Oct 2 10:24:23 1992

Plot 4: Radial Head — Linear CTS vs SPIN PHASE ANGLE (degrees) — Fri Oct 2 10:24:23 1992

Dynamics Explorer Data Analysis Display
(Copy of CRT Screen)

APPENDIX B

JOVIAN BREMSSTRAHLUNG X RAYS: A ULYSSES PREDICTION

J. H. Waite, Jr.[1], D. C. Boice[1], K.C. Hurley[2],
S.A. Štern[1], and M. Sommer[3]

Abstract. The Jovian aurora is the most powerful planetary aurora in the solar system; to date, however, it has not been possible to establish conclusively which mechanisms are involved in the excitation of the auroral emissions that have been observed at ultraviolet, infrared, and soft X ray wavelengths. Precipitation of Iogenic heavy sulfur and oxygen ions, downward acceleration of electrons along Birkeland currents, and a combination of both of these mechanisms have all been proposed to account for the observed auroral emissions. Modeling results reported here show that precipitating auroral electrons with sufficient energy to be consistent with the Voyager UVS observations will produce bremsstrahlung X rays with sufficient energy and intensity to be detected by the Solar Flare X Ray and Cosmic Ray Burst Instrument (GRB) on board the Ulysses spacecraft. The detection of such bremsstrahlung X rays at Jupiter would provide strong evidence for the electron precipitation mechanism, although it would not rule out the possibility of some heavy ion involvement, and would thus make a significant contribution toward solving the mystery of the Jovian aurora.

Introduction

The identity of the precipitating particles involved in Jovian auroral activity is still an open question. In situ observations of the Jovian particle populations during the Voyager 1 and 2 encounters furnished evidence for changes in the radial phase space distribution of energetic heavy ions which are best explained by ion precipitation [Gehrels and Stone, 1983]. However, the energy range of the ion measurements did not go low enough to demonstrate that heavy ion precipitation could provide the power input required to explain the ultraviolet emission intensities. Voyager provided no in situ evidence for electron precipitation; however, indications of electron acceleration in Birkeland currents connected to the auroral zone would only be observable at high latitudes closer to the planet, a region not accessible to the Voyager spacecraft.

Remote sensing observations also present a mixed picture. Soft (0.3-3.0 keV) X ray observations of the Jovian aurora by the Einstein observatory [Metzger et al., 1983] have been used to argue for heavy ion precipitation.

[1]Department of Space Sciences, Southwest Research Institute, San Antonio, TX
[2]Space Sciences Laboratory, University of California, Berkeley, CA
[3]Max-Planck-Institut für Extraterrestrische Physik, Garching, Germany

The energy resolution of the Einstein X ray observatory was not sufficient to distinguish between a bremsstrahlung power law distribution and K-shell emission line spectra from sulfur and/or oxygen. However, based on modeling the K-shell and bremsstrahlung mechanisms and their response within the Einstein telescope, Metzger et al. [1983] inferred that the energy required to produce the observed soft X ray emission by means of electron bremsstrahlung was unreasonably large compared with that required by the K-shell mechanism and thus argued in favor of heavy ion precipitation as the source of Jovian auroral X rays. This conclusion has been substantiated by the recent electron bremsstrahlung calculations of Waite [1991]. On the other hand, attempts at observing extreme ultraviolet emissions from sulfur and oxygen precipitation were unsuccessful [Waite et al., 1988] and suggested that, although heavy ion precipitation may indeed be the source of the soft X rays, heavy ions may not have sufficient energy flux to account for the bulk of the H_2 ultraviolet emissions observed by Voyager [Broadfoot et al., 1981] and IUE [Livengood et al., 1990].

Indeed, the H_2 Lyman and Werner band emission intensities and spectral characteristics of the ultraviolet emissions can be used to set constraints on both the energy flux and energy distribution of the precipitating particles [Livengood et al., 1990]. In this paper these constraints are used in conjunction with modeling techniques to predict the hard X ray fluxes that are expected to be detected at Jupiter by the Solar Flare X Ray and Cosmic Ray Burst Instrument (GRB) as Ulysses makes its closest approach in mid-February of 1992.

Model

The auroral electron distributions as a function of altitude and energy are found by using a two-stream electron transport code modified for Jupiter [Waite et al., 1983] and extended to electron energies of 2 MeV using the relativistic H_2 cross sections of Garvey et al. [1977]. The differential bremsstrahlung cross sections were taken from the work of Koch and Motz [1959] (formulae 3BN and II-6). X ray atmospheric absorption effects were calculated, but were less than 10% at all photon energies above 100 eV for all primary electron beam energies considered. The electron transport model also calculates the electron-induced H_2 ultraviolet band emissions using the most recent cross sections of Ajello et al. [1988] and Shemansky and Ajello [1988] with the most recent corrections for absolute laboratory reference calibration [R. Gladstone, private communication, 1991].

The model also solves the one-dimensional chemical diffusion equations for atomic hydrogen and the hydrocarbon species CH_4, C_2H_2, C_2H_4, C_2H_6, and CH_3, and the major ion species H^+ and H_3^+. The neutral temperature structure adopted in the present study is an equatorial

profile determined from the Voyager ultraviolet spectrometer (UVS) occultation experiments [Festou et al., 1981]. Although auroral energy input is expected to modify this profile, there is at present limited information as to the effects of this input. Furthermore, increases in the auroral thermal structure produce little change in the calculations apart from changes in the relative altitude of the atmosphere. The hydrocarbon density profiles used in this model are consistent with the recent work of Gladstone et al. [1991] and use an eddy diffusion coefficient of 2×10^6 cm^2 s^{-1} at the methane homopause.

The characteristics of the H_2 Lyman and Werner band spectra observed in Jovian auroral emissions are significantly affected by methane and acetylene, which absorb differentially over the H_2 band's spectral range. The measure of this differential absorption is the color ratio, which Livengood et al. (1990) have defined as the ratio of the integrated intensities (I) of two wavelength bands: I(1557-1619Å)/I(1230-1300Å).This ratio can be used to infer the methane column density above the region of peak H_2 band emissions: since methane is a strong absorber in the wavelength range 1230 to 1300Å and not in the range 1557 to 1600Å, a high color ratio indicates a large column abundance of methane. The methane absorption effects are related to the H_2 vertical distribution through the specified eddy diffusion coefficient and thermal structure. Electron energies used in the model to determine bremsstrahlung X ray fluxes are chosen by inputting electron beams into the assumed model atmosphere and then selecting the ones that fit to the observed color ratios for CH_4 absorption.

Uncertainty in determining the primary electron beam energy is introduced by assuming that the equatorial and auroral regions of the atmosphere have the same vertical structure. The present uncertainty hinges on our lack of knowledge about the high-latitude methane vertical structure and for the present we simply use the measured near-equatorial structure inferred from Voyager UVS measurements [Festou et al., 1981]. However, we note that if Ulysses determines a bremsstrahlung X ray photon energy spectrum then it will provide an independent constraint on the precipitating electron energy distribution. Simultaneous ultraviolet observations of the color ratio by an ultraviolet observatory (such as HST) would thereby not only allow us to check our modeling assumptions, but would provide unique information on the polar auroral atmosphere.

Anticipated Ulysses GRB Observations

The GRB instrument on Ulysses consists of two hemispherical shell CsI scintillators coupled to phototubes for measuring X rays in the range of 20 to 150 keV, with time resolution up to 8 ms. A detailed description of the instrument can be found in Hurley et al. [1992]. We have calculated the Ulysses sensitivity to Jovian X rays from data accumulated over the first year of operation. During solar quiet periods, which are characteristic of the majority of the mission, the 18-100 keV background rate of each detector is around 200 counts/second; this arises primarily from the diffuse cosmic X ray background and the Radioisotope Thermoelectric Generator aboard the spacecraft. Using the corresponding count rates in the

individual energy channels, and assuming a 100 minute integration, we obtain the 3 sigma sensitivities given in Table I and shown in Figure 2.

The closet approach of the Ulysses spacecraft to Jupiter will occur on February 8th of 1992. The spacecraft will approach Jupiter over the north polar cap, pass through perijove near 6.3 R_J, and exit the Jupiter system over the southern polar cap. Although Jupiter's trapped energetic particles will preclude observations near the equator, observations over the north and south poles will be possible before and after closet approach.

Results

Model H_2 band calculations have been matched to the statistical information concerning ultraviolet emission intensity and color ratio determined by ten years of IUE observations [Livengood et al., 1990], and the flux and energy distribution of the incoming electrons have been calculated. These calculated electron beams have been used to compute bremsstrahlung X ray fluxes, which serve as the predictive data set for the Ulysses GRB observations.

The specification of the precipitating electron spectrum is of the form $J(E)=J_{op}(E/E_{op}) \exp(-E/E_{op})$, where the parameter J_{op} specifies the differential flux (cm^{-2} s^{-1} keV^{-1}) and E_{op} the characteristic energy (keV) of the precipitating electrons. Since the IUE observations show that both the intensity and the color ratio are strong functions of the S_{III} longitude, we have modeled these observations using three independent sets of primary electron parameters which correspond to ultraviolet observational values at 0, 150, and 180 degrees S_{III} longitude in the northern auroral zone (NAZ). The electron beam parameters and the associated ultraviolet characteristics are given in Table II for the three cases. The color ratio has been calculated at two zenith view angles, 0 and 60 degrees. The effect of doubling the hydrocarbon density (60° zenith view angle) results in a 11 to 19% increase in the color ratio due to differential methane absorption, as discussed above. The calculated variance of the color ratio illustrates the sensitivity of the calculation to the view angle of the ultraviolet observation and gives some idea of the sensitivity of the calculation to the chosen model atmosphere. Values of the H_2 band intensity and color ratio for the three cases have also been spline-fit to produce a model curve which can be compared to the Livengood et al. [1990] IUE observations. The results of that fit are shown in Figure 1. In Figure 1(a), auroral H_2 band intensities have been integrated over the restricted spectral range 1557-1619Å (a rough comparison

TABLE I. Ulysses GRB Sensitivities

Channel No.	Energy Channel (keV)	Sensitivity (Photons cm^{-2} s^{-1} eV^{-1})
1	18.1 - 31.1	9.8×10^{-7}
2	31.1 - 43.5	1.0×10^{-6}
3	43.5 - 56.0	9.3×10^{-7}
4	56.0 - 68.4	7.7×10^{-7}
5	68.4 - 80.9	6.2×10^{-7}

TABLE II. Model Parameters and UV Properties

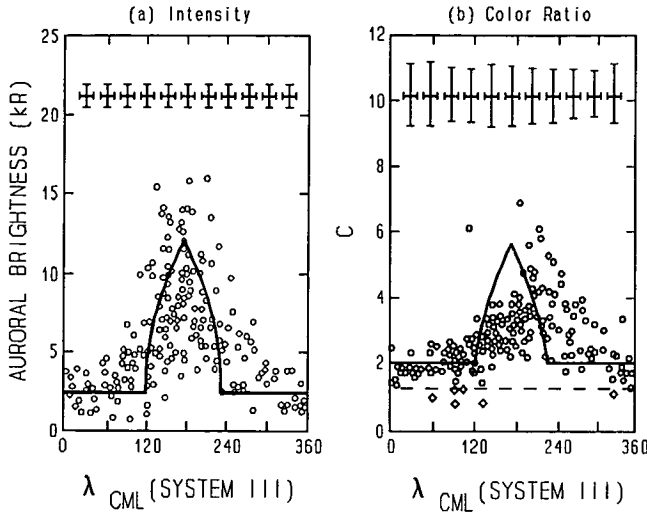|	S_{III} Longitude (degrees)	E_{op} (keV)	Energy Flux (erg cm^{-2} s^{-1})	H_2 Bands (kR)	Color Ratio (zenith angle)
Case 1	0	20	2.8	21.9	1.98(0°) 2.20(60°)
Case 2	150	37	9.8	83.2	4.17(0°) 4.92(60°)
Case 3	180	45	12.1	105.1	5.43(0°) 6.47(60°)

(a) Intensity   (b) Color Ratio

Fig. 1. (a) Intensity and (b) color ratio distribution of the H_2 extreme ultraviolet (EUV) auroral emissions. In Figure 1(a) the H_2 EUV emission intensity in kilorayleighs is integrated over the range 1557-1619 Å. In Figure 1(b) the intensity in the wavelength range 1557-1619 Å has been divided by the intensity in the wavelength range 1230-1300 Å. In (b), the dashed line is the color ratio value for an unattenuated spectrum of H_2 excited by impact of 100-eV electrons; points below this line are plotted as diamonds. The crosses represent the median error bars in longitude and intensity/color ratio for the 60° width centered on each cross. The uncertainty in intensity and color ratio is computed from the camera noise level. The error bars shown here do not include any estimation of possible systematic error as a consequence of erroneous subtraction. The solid lines in both figures are the present model results.
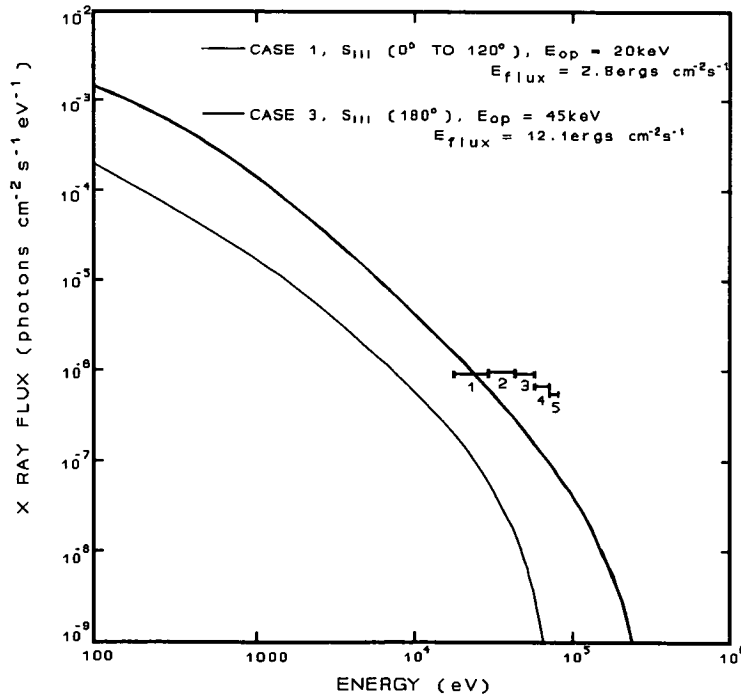
JOVIAN X RAY FLUXES

Fig. 2. The X ray intensity as a function of photon energy for a Jovian auroral source size of 5000 by 10,000 km; viewed from a distance of 10R$_J$. The solid bars marked 1-5 indicate the 3 sigma sensitivities of the five lower GRB channels for a 100 minute integration.

of this restricted intensity/wavelength integration to the total integrated H_2 Lyman and Werner band intensity given in Table II can be obtained by multiplying by 9.1). The fit appears quite good apart from a phase shift of the color ratio in S_{III} longitude; this could be removed by adjusting the characteristic beam energy, E_{op}, a process not warranted given the present uncertainties of the auroral atmosphere. A likely explanation for this effect is that the time-dependent, atmospheric composition is modified by the precipitating electrons, leading to a characteristic lag in S_{III} longitude of the peak hydrocarbon absorption.

Finally, the X ray fluxes that result from the two extreme electron precipitation cases (case 1: 0 to 120 degrees S_{III} longitude in the NAZ and case 3: 180 degrees S_{III} in the NAZ) are shown in Figure 2. The X ray intensity as a function of photon energy is plotted for an auroral zone emission size 5000 by 10,000 km observed from a distance of 10 R_J. Also plotted on the figure is the sensitivity of several of the GRB energy channels for similar viewing conditions and an integration period of 100 minutes.

Conclusions

The results plotted in Figures 1 and 2 indicate that if the ultraviolet auroral emissions are due to precipitating electrons and the Jovian aurora is sufficiently active (this must be determined by simultaneous EUV observations which will be carried out by the Hubble Space Telescope), then the Ulysses GRB experiment should be able to measure the bremsstrahlung X ray spectrum and place firm constraints on both the precipitating electron flux intensity and energy spectrum. Furthermore, observed S_{III} longitude variations in the spectrum can be used in conjunction with the ultraviolet intensity and color ratio values from HST to determine the vertical hydrocarbon structure in the polar stratosphere of Jupiter. On the other hand, if the major precipitating particles are heavy ions, then GRB would detect nothing since its lowest energy channel at 20 keV is above the threshold for both sulfur and oxygen K-shell emissions.

References

Ajello, J.M., D. Shemansky, T.L. Kwok, and Y.L. Yung, Studies of Extreme-Ultraviolet Emission from Rydberg Series of H_2 by Electron Impact, Phys. Rev. A., 29, 636-653, 1984.

Broadfoot, S.K., et al., Overview of the Voyager ultraviolet spectrometry results through Jupiter encounter, J. Geophys. Res., 79, 8259-8284, 1981.

Festou, M. C., S. K. Atreya, T. M. Donahue, B. R. Sandel, D. E. Shemansky, and A. L. Broadfoot, Composition and thermal profiles of the Jovian upper atmosphere as determined by the Voyager ultraviolet stellar occultation experiment, J. Geophys. Res., 86, 5715, 1981.

Garvey, R. H., H. S. Porter, and A. E. S. Green, Relativistic yield spectra in H_2, J. Appl. Phys., 48, 4353, 1977.

Gehrels, N., and E. C. Stone, Energetic oxygen and sulfur ions in the Jovian magnetosphere and their contribution to the auroral excitation, J. Geophys. Res., 88, 5537, 1983.

Gladstone, G.R., M. Allen, Y.L. Yung and J.I. Moses, Hydrocarbon photochemistry in the upper atmosphere of Jupiter (abstract), 23rd Annual meeting of the Division of Planetary Sciences of the American Astronomical Society, 4, Palo Alto, CA, November, 1991.

Hurley, K. et al., The Solar X-ray/cosmic-ray burst experiment aboard Ulysses, Astronomy and Astrophysics Suppl., (in press), 1992.

Koch, H. W., and J. W. Motz, Bremsstrahlung cross-section formulas and related data, Rev. Mod. Phys., 31, 920, 1959.

Livengood, T. A., D. F. Strobel, and H. W. Moos, Long-term study of longitudinal dependence in primary particle precipitation in the north Jovian aurora, J. Geophys. Res.,95, 10,375, 1990.

Metzger, A. E., D. A. Gilman, J. L. Luthey, K. C. Hurley, H. W. Schnopper, F. D. Seward, and J. D. Sullivan, The detection of X rays from Jupiter, J. Geophys. Res., 88, 7731, 1983.

Shemansky, D., M. Ajello, and D.T. Hall, Electron Impact Excitation of H_2: Rydberg Band Systems and the Benchmark Dissociative Cross Section for H Lyman-Alpha, Astrophysical Journal, 296, 765, 1985.

Waite, J. H., Jr., T. E. Cravens, J. Kozyra, A. F. Nagy, S. K. Atreya, and R. H. Chen, Electron precipitation and related aeronomy of the Jovian thermosphere and ionosphere, J. Geophys. Res., 88, 6143, 1983.

Waite, J. H., Jr., J. T. Clarke, T. E. Cravens, and C. M. Hammond, The Jovian aurora: Electron or ion precipitation?, J. Geophys. Res., 93, 7244, 1988.

Waite, J.H., Jr., Comment on "Bremsstrahlung X rays from Jovian Auroral electrons" by D.D. Barbosa, J. Geophys. Res., 96 (A11), 19,529, 1991.

Walt, M., L. L. Newkirk, and W. E. Francis, Bremsstrahlung produced by precipitating electrons, J. Geophys. Res., 84, 967, 1979.

D. C. Boice, S. A. Stern, J. H. Waite, Jr., Department of Space Sciences, Southwest Research Institute, P. O. Box 28510, San Antonio, TX 78228.

K. C. Hurley, Space Sciences Laboratory, University of California, Berkeley, Berkeley, CA 94720.

M. Sommer, Max-Planck-Institut für Extraterrestrische Physik, Garching, Germany

APPENDIX C

Multispectral Observations of the Jovian Aurora

Introduction

The upper atmospheres of the Earth and the outer planets form a screen on which precipitating charged particles, like the electron beam in a television, trace fleeting, but revealing patterns of visible, ultraviolet, infrared, and x ray emissions that offer valuable clues to processes occurring within the planetary magnetospheres. At Earth, years of in situ measurements, as well as ground based observations, have yielded a picture (still fuzzy) where the interaction of the solar wind with the magnetosphere of the Earth provides a complex path for the storage and release of energy during magnetic substorms; the ultimate manifestation of terrestrial auroral processes. More recent global imaging of substorm events from high above the Earth (> 3.5 R_e) by Dynamics Explorer have made a unique contribution towards understanding the global and temporal evolution of such auroral events by providing a morphological perspective and by providing the crucial observational link that allows the separation of spatial and temporal variations inherent in the interpretation of in situ data. A similar role was played by the Hubble Space Telescope (HST) during the recent encounter of Ulysses with Jupiter February, 1992 in helping to define a new paradigm in Jovian auroral physics. The old paradigm portrayed Jupiter's magnetosphere as totally dominated by internal processes (ie. Io related tori, heavy ions, etc.) where energetic heavy ion precipitation in the inner magnetosphere was solely responsible for the observed auroral phenomena. Ulysses and HST portray a more Earth-like paradigm where electron acceleration in the outer magnetosphere near the boundary with the solar wind plays a distinct role in the formation of auroral hot spots, yet energetic heavy ions also enter into the picture [this paper; Dols et al., 1992] (similar to the role of the energetic ions from the terrestrial ring current during magnetic substorms). These heavy ions as a result of excitation during their transit through the atmosphere produce the x ray emissions observed in Roentgensatellit (ROSAT) x ray energy spectra.

The ultraviolet spectrometers on the Voyager 1 and 2 spacecraft [Sandel et al., 1979; Broadfoot et al., 1981] and the International Ultraviolet Explorer (IUE) spacecraft [Clarke et al., 1980; Yung et al., 1982] observed intense H_2 Lyman and Werner band emissions from the Jovian atmosphere at high latitudes, thus providing evidence for auroral particle precipitation at Jupiter. Observations in the infrared [Caldwell et al., 1980; 1983] showed spatial dependencies similar to those at ultraviolet wavelengths. X ray emissions were seen by the High Energy Astronomical Observatory 2 (Einstein) in the Jovian auroral zone [Metzger et al., 1983]. Taken together, these observations provide indications of an aurora more than 100 times more powerful (>10^{13} Watts) than Earth's, which has a strong influence on the high-latitude structure, dynamics, and energetics of the upper atmosphere of Jupiter.

Earlier observations of the Jovian x ray aurora [Metzger et al., 1983] and in situ measurements of energetic oxygen and sulfur [Gehrels and Stone, 1983] indicated that energetic sulfur and oxygen were precipitating into the high-latitude Jovian atmosphere and were largely responsible for the observed ultraviolet auroral emissions. Building on the earlier work concerning electron aurora [Waite et al., 1983], Horanyi et al. [1988] developed a quantitative

1

model of the interaction of energetic oxygen ions and atoms with an H_2, H atmosphere. The model results indicated that sulfur and oxygen emissions in the ultraviolet at 1256 and 1304 angstroms should be detectable with the IUE UV telescope. Subsequent observations and analysis, however, showed no detectable emission at 1304 angstroms and an uncertain detection at 1256 angstroms [Waite et al., 1988]. This lead Waite and colleagues to conclude that the bulk of the observable UV auroral emissions are probably due to electrons and that the ions that do precipitate are quite energetic (>300 KeV/nucleon) and are responsible for the x ray emissions, but do not make a significant contribution to the ultraviolet auroral emissions.

The conclusion of Waite et al. [1988] was not readily endorsed by the Jupiter magnetospheric community, which continued to embrace the dominant role of heavy ion precipitation as a source for the Jovian aurora. Until recently little new observational information was available to allow a re-examination of the energetic ion paradigm. However, the recent Ulysses encounter with Jupiter and the coordinated HST auroral imaging campaign reported in this paper present new evidence for an expanded role for electrons and association of the energetic electron source with the Jovian magnetopause boundary. In addition, ROSAT observations confirm the role of energetic heavy ions in x ray production, but suggest that the source is limited to energies greater than 300 KeV/ nucleon and as suggested by Waite et al. [1988] comprises only a fraction of the measured ultraviolet emission. Thus, a new paradigm of Earth-like auroral processes appears to be emerging from these exciting new results.

Hubble Space Telescope Faint Object Camera Images: Observations and Analysis

Three separate HST investigations were scheduled and carried out with the FOC using three different filter sets. They were: 1) Caldwell et al. (F140W & F152M), 2) Paresce et al. (F120M &F140W), and 3) Stern et al. (F130M & F140W). The observations were obtained from February 6-9, 1992 in the four days surrounding the Ulysses spacecraft's closet approach to Jupiter. The images reported here are from the Stern, McGrath, Waite, Gladstone, and Trafton investigation using the FOC in a f/96 512 by 512 pixel mode (F96N512) with filters F130M and F140W that have a peak spectral response near 1280 angstroms. The field-of-view was 11 x 11 arcseconds and the exposure time for each of the eight images was 18 minutes. The center of the field-of-view was offset 20 arcseconds toward the appropriate Jupiter rotational pole during each observation with a pointing accuracy of approximately 1 arcsecond. For a point of reference Jupiter's polar radius during the time of these observations was approximately 20.54 arcseconds. A summary of the images obtained is shown in Table 1 where we have listed the time of observation, the S_{III} longitude of the central meridian at the midpoint of the observation, the pole observed, the intensity of noticeable features in the image, the emission area, and a rough estimate of the range of the emission power (taking into account the low signal to noise ratio of the data, the difficulty in determining the physical area of the emission, and the uncertainties due to atmospheric absorption).

The determination of the auroral emission power requires that a convolution of the FOC wavelength dependent quantum efficiency (QE) and filter response functions be convoluted with

the auroral H, H_2 spectrum. This was accomplished by modeling both the altitude dependent Lyman alpha and H_2 Lyman and Werner production rate profiles [Waite et al., 1983] assuming a low latitude hydrocarbon vertical distribution [Gladstone and Skinner, 1989] and a precipitating electron spectrum consistent with those observed by Ulysses in the outer magnetosphere [Lanzerotti et al., 1992] and extended down to energies of 20 KeV (below the detector threshold of 44.9 KeV) with the same power law slope in the distribution. The extension to lower electron energies was performed to match the H_2 band color ratio (a measure of the lower energy extent of the precipitating electron distribution for a specified methane vertical profile) generally observed in the Jovian auroral zone [Yung et al., 1980; Waite et al., 1988]. These production rate values were then used as input to a radiative transfer code [Gladstone and Skinner, 1988] (for output see Figure 1a) and then passed through an FOC QE/filter response to produce the synthetic spectrum seen in Figure 1b. As you can see the F130M F140W filter pair responds to both Lyman alpha and Werner band emission near 1280 angstroms, whereas the Paresce images are more sensitive to Lyman alpha and the Caldwell images to Lyman emission near 1580 angstroms. The latter wavelength region is less susceptible to methane absorption, thus it's specification in the upper wavelength range of the Yung et al. [1980] H_2 band color ratio:

CR= Intensity(1557-1619 angstroms)/Intensity(1230-1300 ang.)

A comparison of the relative spectral responses of the three different filter combinations is shown in Table 2. In order to verify that this approach for determining the integrated auroral flux from the limited bandpass 130M 140W combination was not overly sensitive to the assumed methane vertical profile or to the assumed electron energy spectrum used in the modeling we repeated the QE/filter convolution with a measured IUE Jovian auroral spectrum and got the same result to within 20%. We then used the predicted FOC count rates and compared them to the measured rates along with constants that define the telescope's effective area to estimate the power influx levels required to produce the observed auroral emissions (shown in Table 1).

Two images of the north auroral zone (NAZ) and six images of the south auroral zone (SAZ) were obtained over the 4 day span. Five images (1 of the NAZ, 4 of the SAZ) showed emission (>1 sigma) above the image dark count. These five images are shown in Figures 2a and 2b. The image has been processed using a 10 pixel box car average and the color bar has been dynamically stretched to provide a common intensity representation from image to image while at the same time maximizing contrast in the low signal to noise level images. The average background count rate in the five processed images was 0.598 +/- 0.088 counts per pixel, whereas the count rate on the planet without auroral emission was 0.0654 +/- 0.094 counts per pixel. This suggest, as the images indicate, that there is no statistically visible planet limb to aid in interpreting the planetary coordinates. The limb and auroral zone overlays that are shown are determined by constructing a planetary coordinate grid and two sets of auroral zones: 1) L=6, associated with the Io plasma torus, and 2) L=infinity, associated with the last closed magnetospheric field line using the O_4 magnetic field model [Acuna and Ness, 1976] and an IDL program written by Dr. Tim Livengood to process IUE spectra from Jupiter. The finite spread to the auroral zones shown are simply due to the rotation of the planet during the 18 minute exposure. Peak count rates on the images lie between 0.88 and 1.67 counts per pixel which

corresponds to auroral intensities between 20 and 50 kiloRayleighs (kR), yet the low sensitivity of the dual filter FOC combination sets a detection threshold range between 10 and 20 kR. As such only the brighter auroral features are visible in the images and low emission intensities over large areas can mask large uncertainties in the auroral power (See Table 1; image features 101b, 101c, 302b, and 402b where an attempt has been made to estimate the emission uncertainty associated with diffuse emissions over large areas. The selected regions are shown in Figure 3 where a 10 by 10 block average representation of the image with a box overlay designating the selected areas are shown and Table 3 where the average count values and their associated uncertainties are listed.)

The NAZ image (image #101 in Table 1) shows a bright central feature near the Central Meridian Longitude (CML= 163-173 degrees S_{III} longitude) and therefore a reasonable estimate of the S_{III} longitude of the emission feature can be estimated and lies between 160 and 173 degrees. The bifurcated nature of the source can be explained by either spatial (5 degrees of longitude) or temporal (10 minutes, due to planetary rotation during the exposure) variability in the source. The bright source location (image #101a) is most consistent with a middle magnetospheric source (halfway between L=6 and the last closed magnetospheric field line), but a pointing uncertainty of about 1 arcsecond (the size of the marker for celestial N and E) spans the range of auroral zones considered and makes the designation tentative at best. Some weaker emission (image #101b) poleward and westward of the central bright spot is just barely visible above the background as is the area (#101c) to the east of the bright central spot. These areas may represent a weaker "polar oval" emission that is more clearly seen at longer wavelengths in the images of Caldwell et al. (EOS,??). The other NAZ image (#102) suffers from a high noise level that negates meaningful analysis.

The first SAZ image is (image #201 from Table 1). In this image most of the emission appears to lie along the limb of the planet, thus making it difficult to estimate the longitudinal position and intensity of the emission. The CML of this image is 43 degrees S_{III}. Most of the emission appears to lie near a longitude of 180 degrees (#201a, westward edge of auroral zone), but another weaker (?) zone appears near 0 degrees (#201b, eastward edge of the auroral zone). However, image #202 taken 1 hr 27 mn later at a CML longitude of 95 degrees shows emission from the center of the imaged auroral zone (near 100 degrees) and suggests that significant changes in the auroral zone morphology occurred in the intervening time period. The extent of the limb emissions are most consistent with an auroral zone size which corresponds to the boundary of the last closed field lines (ie., maps to near the magnetopause boundary). The intensities listed in Table 1 for this image are uncertain due to the presence of limb brightening effects.

The image pair 301 302 provide information about the temporal variability of the auroral emissions. Image #301 (CML=5 degrees) shows no detectable emission above the background. Whereas, image #302 (CML=56 degrees) shows a bright emission feature between 20 and 30 degrees; a region that should have been clearly visible if present 1 hr 28 mn earlier in image #301. This suggest over a factor of three variation in the auroral intensity during the time period spanned by these two images. Image #302 is also particularly interesting from a Ulysses

encounter point of view, since at the time of the image the HISCALE experiment [Lanzerotti et al., 1992] had just been turned on after closet approach and was observing precipitating energy fluxes of electrons on the order of 1 erg cm^{-2} s^{-1} (~20 kR of emission corresponding to light blue areas just above the background) at the dusk edge of the planet (S_{III}~305 degrees, L~16). Although the conjugate auroral point is just off the field of view of the image a duskward extension of the diffuse auroral emission seen surrounding the central bright spot in an auroral band at L>16 is of a consistent brightest and location to correspond to the measured electrons of HISCALE. Again as in image 201 the auroral zone is more consistent with a mapping to L>15, yet here again pointing uncertainties must be carefully considered. Once again as in image #101 the complex structure of the central bright emission features can be explained by a combination of temporal and spatial structure of the auroral precipitation zones. As a matter of fact in image #302 some of the structure must be spatial because the large separation (>1 arcseconds) of hot spots cannot be explained by rotation of a time variable source alone.

Finally the image pair 401 402 again illustrate both the temporal and spatial variability of the source. No detectable emission above background is seen in image #401 (CML=350-360 degrees), but 1 hr 26 mn later an emission (image #402a) appears near 300 degrees CML; a longitude range that should have been visible in image #401. The magnetic latitude in 402 is again more consistent with auroral emission that maps to the magnetopause boundary than with emission that maps to the Io plasma torus.

HST FOC Images: Discussion

A major consideration in placing these HST FOC images in the context of past Voyager UltraViolet Spectrometer (UVS) and International Ultraviolet Explorer (IUE) observations is the low signal to noise ratio of the images and the resulting sensitivity threshold between 10 and 20 kR of emission over large areas of the high latitude region which would not be visible above the background. Clearly these images are a high spatial resolution tracer of the variations in the auroral bright spots and not as good of an indicator of the more diffuse auroral emission or correspondingly of the total auroral power output. Integrated power numbers for the input power required to produce these bright emissions range from 10^{10} to 10^{12} Watts in both the SAZ and NAZ. However, if we assume that a 20 kR band from 65 to 85 degrees may exist below the detection limit of the FOC then up to 4 x 10^{13} W of input power may be present, but unaccounted for by the present observations. This also would imply that less than 10% of the emission is found in the bright spots, whereas Herbert et al.'s [1987] analysis of the Voyager data suggest that between 20 and 30% of the emission is concentrated in the bright auroral emission regions. Furthermore, Herbert et al. [1987] give estimates of the emitted power (in their Table 2) which can be used to estimate the input power using the emissions efficiencies given by Waite et al. [1983]. Their results give values for the total auroral power input for Voyager 1 inbound of 1.2 x 10^{14} Watts and for the outbound 4 x 10^{13} Watts and an estimate for Voyager 2 of 1.1 x 10^{14} Watts. Livengood [1991] has performed an extensive analysis of the IUE Jovian aurora data set. Using the information from Figure 5.9 of Livengood [1991] and the modeled emission efficiencies from Waite et al. [1983] we obtain an average auroral H, H_2 emission power of 4.4 x 10^{12} Watts (both poles) and an input power of 2.4 x 10^{13} W with a one sigma variance of ~1

5

x 10^{13} Watts and individual data points that show up to a factor of six variation in the emitted power over the span of less than one month. The limited data set of Livengood [1991] spans over 10 years with relatively greater sampling since 1988, but there are no indications of a long term trend in the auroral power output. Placing the measured and inferred auroral power output of the FOC images in the context of the UVS and IUE data suggest that: 1) the majority of the emitted auroral power is in diffuse and weak features below the sensitivity threshold of the FOC, 2) the auroral output power during the Ulysses encounter was in the range of it's observed average as determined by IUE (1 to 3 x 10^{13} Watts), and 3) the aurora is randomly time variable on time scales as short as 10 minutes (given a temporal interpretation of the bifurcation of the bright spot in image #101), and certainly varies by over a factor of three in brightness on time scales of hours.

The UVS and IUE data sets also indicate a systematic variation of the intensity of the auroral emissions in both the NAZ and SAZ as a function of S_{III} longitude. Although these bright regions are identified in the FOC data set (image #101 for the NAZ, central bright spot at ~170 degrees; image #302 for the SAZ, central bright spot at ~25 degrees), the considerable spatial and temporal variation that occurs in time spans of less than two hours in the set of eight FOC images reported here suggest a much more complex pattern of variability (at least for the brightest auroral emissions) and further suggest that part of the systematic variance from IUE and UVS may be due to geometrical considerations of a large spectrometer slit viewing an increasing area of diffuse and distributed auroral emission at certain preferred S_{III} longitudes.

Information on the spectral variations of the Lyman alpha and Lyman and Werner band systems cannot be inferred from the single filter set used in the reported FOC images. As a result, information about the H_2 band color ratio as a function of longitude reported by both IUE and UVS, which gives information on the input particle energy spectrum and/or the changes in the hydrocarbon atmosphere, cannot be compared at present. However, by mixing the different images from the three sets of observations it may be possible to draw some conclusions about systematic variations in the emission spectrum (see Table 3). The one caveat is the high degree of variability will make any spectral comparison from one image to the next hard to quantify.

The most exciting new piece of information comes from the high spatial resolution that can be obtained from HST. The small bright discrete sources seen in the data set put obvious constraints on the magnetospheric processes responsible for the precipitating particles. This patchy and discrete structure is also present in the observed high-latitude magnetospheric particle populations observed by the HISCALE particle detector on the Ulysses spacecraft [Lanzerotti et al., 1992]. Furthermore, the location of the discrete features in latitude (although individually accurate to one arcsecond due to pointing uncertainties) collectively are consistent with a precipitating particle origin in the middle (NAZ) or outer (SAZ) magnetosphere, which is again consistent with the measurement by HISCALE of precipitating electrons in the middle and outer magnetosphere. The limited data available, however, make a comparison to Voyager UVS derived auroral zone [Herbert et al., 1987] difficult to carry and further HST observations are needed to verify the present result. The inference to be drawn from this information is that the Jovian aurora is more Earth-like than previously thought and that acceleration of electrons carrying field-aligned currents in the middle and outer magnetosphere may be largely responsible for the

discrete auroral emission features seen by HST in the southern auroral zone.
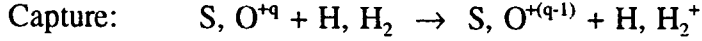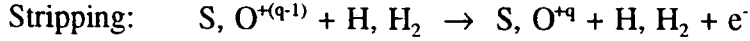
ROSAT Observations

The ROSAT Position Sensitive Proportional Counter (PSPC) acquired nine data segments between April 23, 1991 and April 25, 1991 that have the Jupiter disk within the field of view. The times for each segment are listed below in Table 4. Due to the low count rates in each of the individual data segments the portion of the image which contained the disk of Jupiter (with a factor of two spatial margin) was extracted from each of the nine data segments, individual background subtractions using clear sky were performed, and the resulting data was combined into a single spectra. Therefore no information exist about the possible variation of the spectra as a function of Jupiter rotational phase. However, the single spectrum has been thoroughly analyzed in the context of a best fit bremsstrahlung and a best fit two emission line model. The data along with the results of these best fit models are shown in Figure 4. Please note that the model fits have been convolved with the proper energy resolution and energy dependent quantum efficiencies to allow a comparison with the extracted PSPC data. Therefore, the data shown are not to be interpreted as spectra, but as spectra convoluted with the PSPC response function. Although, the signal to noise is low in the data set due to the small amount of on-Jupiter observation time in the present data set, the two line model is clearly a better fit with a chi square that is over a factor of two better than the best fit bremsstrahlung model (and also a factor of two better than the best power law fit which is not shown in the figure).

ROSAT Discussion

The total x ray power inferred from the analysis is 1.3 to 2.1 x 10^9 Watts depending on whether the model fit assumed is the two line or the bremsstrahlung, respectively. This is within a factor of three of the 4 x 10^9 Watts reported from the Metzger et al. [1983] Einstein x ray observations. The observed comparison is within variations that are associated with changes in the ultraviolet auroral output [Livengood, 1991]. Furthermore, in agreement with Metzger et al. we conclude that from bremsstrahlung x ray modeling that the model efficiency (5.6 x 10^{-7} ; Waite, 1991) suggests that over 3 x 10^{15} Watts of auroral electron precipitation would be required to produce the observed x ray emission from an electron bremsstrahlung source. However, the factor of two better energy resolution available with ROSAT (as compared to Einstein) also allows a spectral interpretation of the results. This data as shown in Figure 4 suggests that a two line emission model produces a better fit (by a factor of two in chi square) than does the best bremsstrahlung fit. Yet the line model fit has two components, a narrow component near 0.2 KeV and a broader component centered at 0.9 KeV, which are not consistent with the Metzger et al. interpretation of S and O K-shell emission at 2.3 and 0.52 KeV, respectively. Reference to the soft x ray emission tables of Raymond and Smith [1977] does indicate a series of S(VII) recombination lines near 0.2 KeV and a series of O(VII) recombination lines near 0.9 KeV which are strong candidates for explaining the observed emissions (see Figure 5). The production of these emission lines occurs as a result of recombination lines that are produced from the slowing of the energetic ion beam as it enters the Jupiter upper atmosphere.

Charge state equilibrium of the ion beam in the atmosphere results from competition between electron capture and stripping which are charge state and energy dependent.

Stripping: S, $O^{+(q-1)}$ + H, H_2 $\rightarrow$ S, O^{+q} + H, H_2 + e^-

Capture: S, O^{+q} + H, H_2 $\rightarrow$ S, $O^{+(q-1)}$ + H, H_2^+

We estimate that in the electron capture process 10% of the reaction exothermicity goes into the excitation of recombination lines. If the initial charge states are S(VII) and O(VII) the resulting emission is in the soft x ray wavelength regime.

Recombination excitation:

$$S(VIII), O(VIII) + H, H_2 \rightarrow S(VII), O(VII)^* + H, H_2^+$$

$$S(VII), O(VII)^* \rightarrow S(VII), O(VII) + x\ ray$$
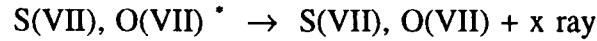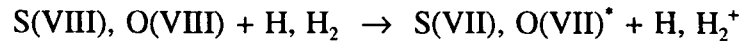
The high charge states necessary to produce these emissions are the result of the incident ion beam energy and the fact that electron stripping and capture processes result in a rapid charge state equilibrium being established as the beam encounters the upper atmosphere. This point is illustrated (Figure 6) for energetic oxygen where we have presented the equilibrium fraction of the various charge states as a function of beam energy (results from private communication with T. E. Cravens, 1992). The figure indicates that an O(VII) charge state will occur for all ions that enter the atmosphere with an energy greater than ~700 KeV per amu. That such ions exist in the Jupiter magnetosphere and probably precipitate between L=7 and 10 has been demonstrated using Voyager data by Gehrels and Stone [1983]. They estimate that between 10^{12} and 10^{13} Watts of oxygen and sulfur with energies greater than 700 KeV per amu is precipitating into the Jupiter. This implies that an efficiency of 0.01 to 0.1% is required from x ray recombination processes to explain the present x ray aurora in a manner consistent with the observed loss of energetic oxygen and sulfur by Voyager [Gehrels and Stone, 1983]. Such an efficiency appears to be quite reasonable in the context of the modeling of energetic oxygen aurora at Jupiter by Horanyi et al. [1988] and detailed modeling calculations are now in progress.

However, we further note that as pointed out by Gehrels and Stone [1983] the observed energetic ion precipitation does not contain sufficient power to explain the observed ultraviolet aurora and extrapolations to 40 KeV per amu are required to supply this additional power. Such an extrapolation is not necessary to explain the observed x ray emissions. We therefore, conclude that in light of the HST Ulysses results, both electrons and ions play a role in the Jupiter auroral emissions, but that the bulk of the ultraviolet emissions (and thus a major portion of the power input) comes from electron processes, which result from processes in the outer magnetosphere and not from energetic ions precipitating from the middle magnetosphere. Such a scenario forms the new paradigm of the Earth-like aurora at Jupiter.

References

Acuña, M. H., and N. F. Ness, Results from the GSFC fluxgate magnetometer on Pioneer 11, in *Jupiter*, edited by T. Gehrels, p. 830-847, University of Arizona Press, Tucson, 1976.

Broadfoot, A. L., et al., Overview of the Voyager ultraviolet spectrometry results through Jupiter encounter, *J. Geophys. Res.*, *86*, 8259-8284, 1981.

Caldwell, J., A. T. Tokunga, and G. S. Orton, Further observations of 8 μm polar brightenings of Jupiter, *Icarus*, *53*, 133-140, 1983.

Caldwell, J., A. T. Tokunga, and F. C. Gillett, Possible infrared aurorae on Jupiter, *Icarus*, *44*, 667-675, 1980.

Caldwell, J., *EOS*???

Clarke, J. T., H. W. Moos, S. K. Atreya, and A. L. Lane, Observations from Earth orbit and variability of the polar aurora on Jupiter, *Astrophys. J. (Lett.).*, *241*, L179-182, 1980.

Dols, V., J. C. Gerard, F. Paresce, R. Prange, and A. Vidal-Madjar, Ultraviolet imaging of the Jovian aurora with the Hubble Space Telescope, in press *GRL*, 1992.

Gehrels, N., and E. C. Stone, Energetic oxygen and sulfur ions in the Jovian magnetosphere and their contribution to the auroral excitation, *J. Geophys. Res.*, *88*, 5537-5550, 1983.

Gladsstone, G. R., and T. E. Skinner, Spectral analysis of Jovian auroral emissions, in *Time-Variable Phenomena in the Jovian System*, M. J. S. Belton, R. A. West, and J. Rahe, Eds., NASA SP-494, Washington, D. C., 221-228, 1989.

Herbert, F., B. R. Sandel, and A. L. Broadfoot, Observations of the Jovian UV aurora by Voyager, *J. Geophys. Res.*, *92*, 3141-3154, 1987.

Horanyi, M., T. E. Cravens, and J. H. Waite, Jr., The precipitation of energetic heavy ions into the upper atmosphere of Jupiter, *J. Geophys. Res.*, *93*, 7251-7271, 1988.

Lanzerotti, L. J., T. P. Armstrong, R. E. Gold, K. A. Anderson, S. M. Krimigis, R. P. Lin, M. Pick, E. C. Roelof, E. T. Sarris, G. M. Simnett, C. G. Maclennan, H. T. Choo, and S. J. Tappin, Hot plasma environment at Jupiter: Ulysses results, in press *Science*, 1992.

Livengood, T. A., R. M. Prangé, G. E. Ballester, and H. W. Moos, Exceptional variability of the Jovian ultraviolet aurora of December 1990: Primary particle energy and identity?, *EOS Trans. AGU*, *72*, 185, 1991.

Metzger, A. E., D. A. Gilman, J. L. Luthey, K. C. Hurley, H. W. Schnopper, F. D. Seward, and J. D. Sullivan, The detection of X-Rays from Jupiter, *J. Geophys. Res.*, *88*, 7731-7741, 1983.

Raymond, J. C., and B. W. Smith, Soft x ray spectra of a hot plasma, *App. J. Suppl.*, *35*, 419-439, 1977.

Sandel, B. R., et al., Extreme ultraviolet observation from Voyager 2 encounter with Jupiter, *Science*, *206*, 962-966, 1979.

Waite, J. H., Jr., Comment on "Bremsstrahlung X rays from Jovian auroral electrons" by D. D. Barbosa, *J. Geophys. Res.*, *96*, 19,529-19,532, 1991.

Waite, J. H., Jr., J. T. Clarke, T. E. Cravens, and C. M. Hammond, The Jovian aurora: Electron or ion precipitation?, *J. Geophys. Res.*, *93*, 7244-7250, 1988.

Waite, J. H., Jr., et al., Electron precipitation and related aeronomy of the Jovian thermosphere and ionosphere, *J. Geophys. Res.*, *88*, 6143-6163, 1983.

Yung, Y. L., et al., H_2 fluorescence spectrum from 1200 to 1700Å by electron impact: Laboratory study and application to Jovian aurora, *Astrophys. J. (Lett.).*, *254*, L65, 1982.

Yung, Y. L., and D. F. Strobel, Hydrocarbon photochemistry and Lyman alpha albedo of Jupiter, *Astrophys. J.*, *238*, 395-402, 1980.

Figure Captions

Figure 1a. Model Jovian auroral spectrum of the H Lyman alpha and H_2 band emissions.

Figure 1b. The convolution of the model spectrum with the wavelength dependent filter and quantum efficiencies response curves for the HST FOC F130M/F140W.

Figure 3. Ten by ten block averaged representation of the full set of HST FOC images with boxes indicating positions of intensity information extraction.

Figure 4. Combined ROSAT PSPC photon energy spectrum and the model curves for a best fit two line model and a best fit bremsstrahlung model convoluted with the detector response function.

Figure 5. Two line model fit and the wavelength location and relative intensity of known recombination emission lines from S(VII) and O(VII).

Figure 6. Equilibrium fraction for O^{+q} (q = 0, 8) charge state distributions as a function of ion energy.

Table 1. HST Jovian Auroral Observations

#	DATE	TIME(UT)	CML(S_{III})	POLE	Intensity(kR)	Area("^{2})	Power(W)*
101a	2/6/92	2:40	168	North	34 +/- 23	2.9	5×10^{10} - 7×10^{11}
101b	2/6/92	2:40	168	North	13 +/- 14	2.8	0 - 5×10^{12}
101c	2/6/92	2:40	168	North	31 +/- 34	1.1	0 - 2×10^{13}
102	2/6/92	4:08	222	North	High Noise	--	---
201a	2/7/92	9:07	43	South	12 +/- 11	4.8	1×10^{10} - 5×10^{11}
201b	2/7/92	9:07	43	South	24 +/- 18	2.5	2×10^{10} - 5×10^{11}
202	2/7/92	10:34	95	South	49 +/- 30	1.7	1×10^{11} - 5×10^{11}
301	2/8/92	23:46	5	South	Low Signal	--	---
302a	2/9/92	1:11	56	South	26 +/- 21	2.6	1×10^{10} - 5×10^{11}
302b	2/9/92	1:11	56	South	8 +/- 16	2.1	0 - 4×10^{12}
401	2/9/92	9:24	355	South	Low Signal	--	---
402a	2/9/92	10:50	47	South	41 +/- 28	1.8	2×10^{10} - 1×10^{12}
402b	2/9/92	10:50	47	South	22 +/- 24	1.6	0 - 1×10^{13}

* Range limits include not only 1 sigma measurement uncertainties, but also a factor of 2 uncertainty due to unaccounted for atmospheric absorption, a factor of 2-4 increase from the optical defects of HST which depends on the size of the emission region, and an upper limit to the size of the emitting area

Table 2. Spectra for Caldwell, Stern, and Paresce

BAND	CALDWELL (F140W, F152M)	STERN (F130M, F140W)	PARESCE (F120M, F140W)
Lya	0.034	0.340	0.828
1230-1650	0.962	0.648	0.149
1230-1300	0.015	0.385	0.106
1557-1619	0.290	0.010	0.004
Total (cps/pixel)	1.64E-5	6.21E-6	1.29E-5

Table 3. HST FOC Intensity Determination

DESIGNATED IMAGE BLOCK		IMAGE COORDINATES [X1:X2, Y1:Y2]	AVERAGE COUNTS AND VARIANCE (per pixel)
Image 101	101a	[16:23, 14:23]	0.95±0.21
	101b	[10:16, 28:38]	0.74±0.11
	101c	[31:35, 4:10]	0.73±0.10
	bc1(101) [off planet]	[5:13, 3:13]	0.63±0.09
	bc2(101) [on planet, no aurora]	[34:44, 34:44]	0.61±0.09
Image 102	no analysis attempted due to high noise level		
Image 201	201a	[10:18, 25:38]	0.90±0.16
	201b	[36:42, 2:11]	0.91±0.12
	bc1(201)	[4:14, 4:14]	0.62±0.08
	bc2(201)	[25:35, 25:35]	0.70±0.10
Image 202	202	[20:26, 22:28]	0.88±0.14
	bc1(202)	[5:15, 5:15]	0.56±0.09
	bc2(202)	[30:40, 30:40]	0.60±0.09
Image 301	no analysis attempted due to low signal level		
Image 302	302a	[29:37, 7:14]	1.00±0.16
	302b	[24:29, 20:29]	0.83±0.12
	bc1(302)	[5:15, 5:15]	0.66±0.09
	bc2(302)	[30:40, 30:40]	0.77±0.11
Image 401	no analysis attempted due to low signal level		
Image 402	402a	[29:37, 4:9]	0.85±0.12
	402b	[24:29, 17:24]	0.71±0.10
	bc1(402)	[5:15, 5:15]	0.52±0.09
	bc2(402)	[30:40, 30:40]	0.59±0.08

Table 4. Segment Times

START (UT)		STOP
4/23/91	12:52:32	13:01:55
4/23/91	22:03:42	22:31:58
4/24/91	03:11:37	03:26:58
4/24/91	12:51:27	13:00:54
4/24/91	19:00:44	19:12:41
5/24/91	03:10:28	03:24:53
5/24/91	11:15:52	11:23:17
5/24/91	12:42:06	12:59:11
5/24/91	17:22:04	17:40:20
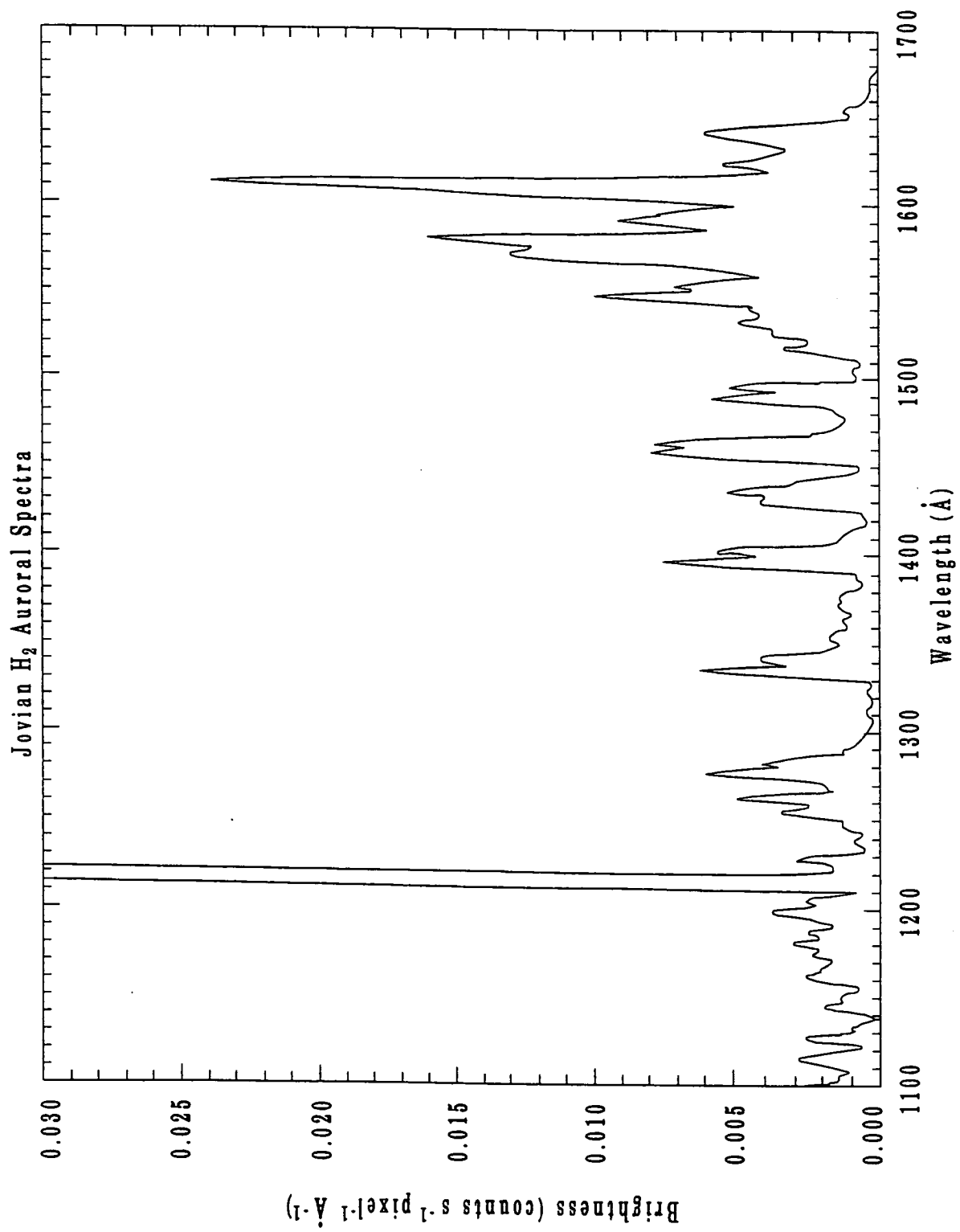
Figure 1a
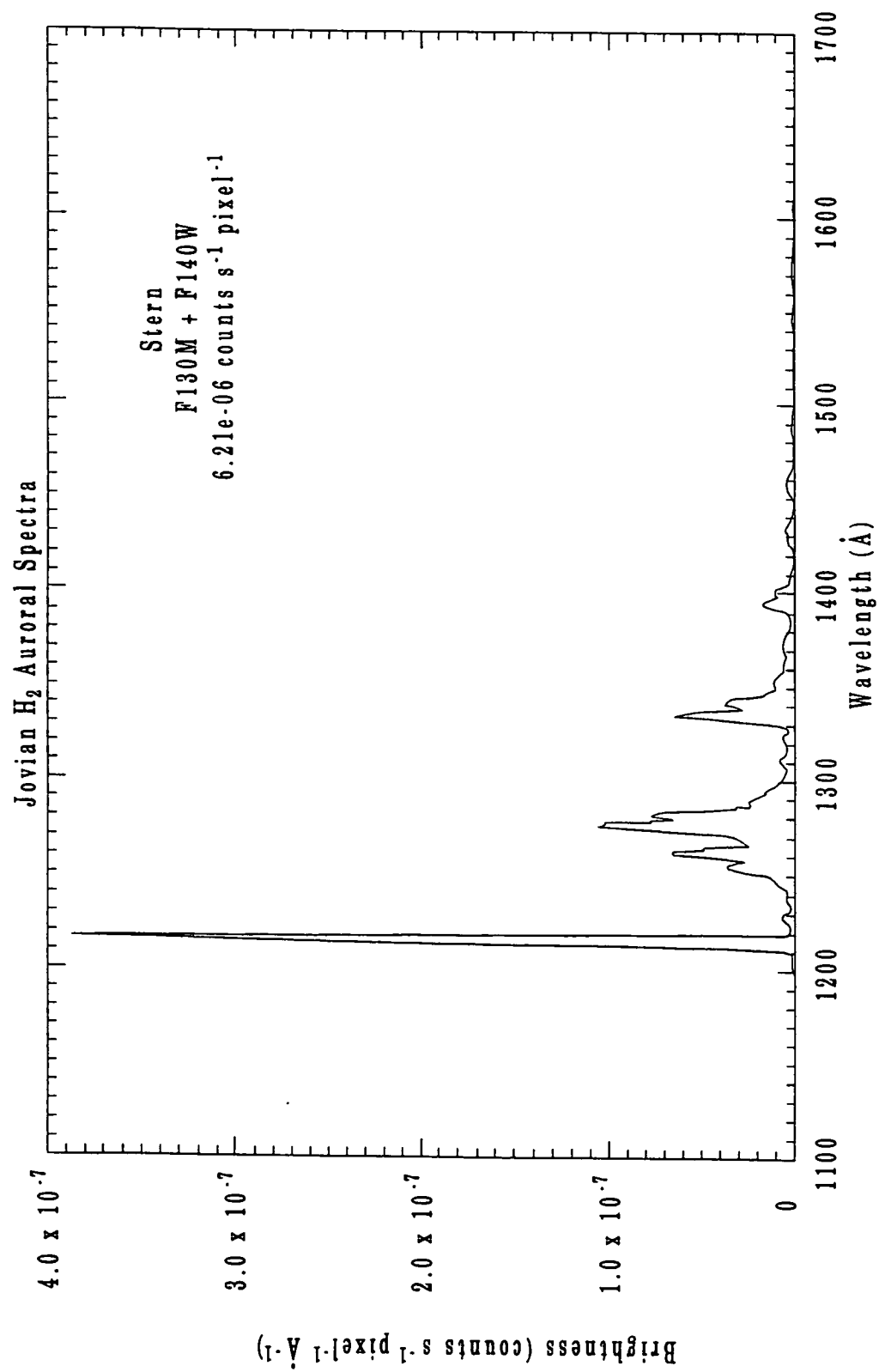
Figure 1b
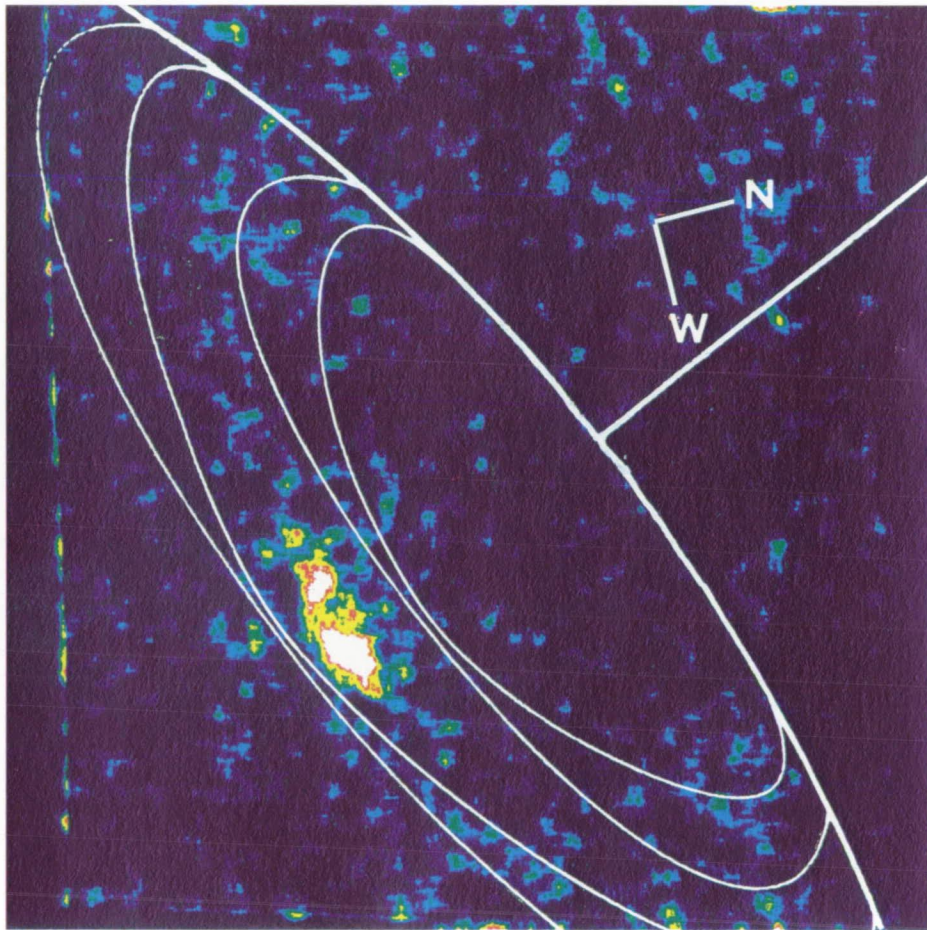
101

Figure 2a. Reduced HST FOC image of the north pole showing bright auroral features and shading that indicate Jovian magnetic coordinates for Io plasma torus auroral zone low latitude circle and magnetopause auoroal zone smaller inner circle.
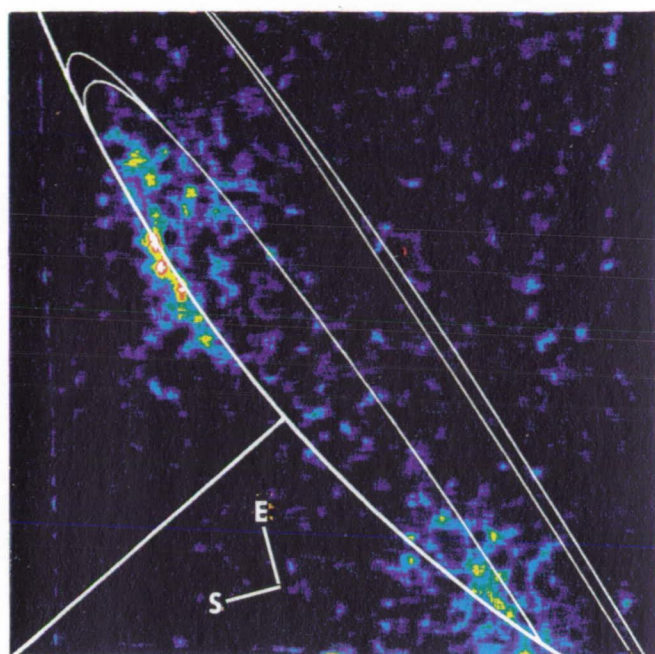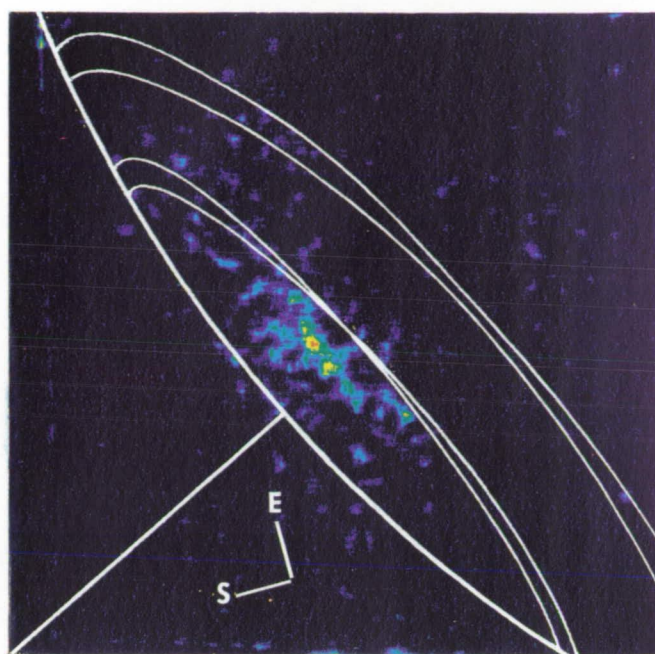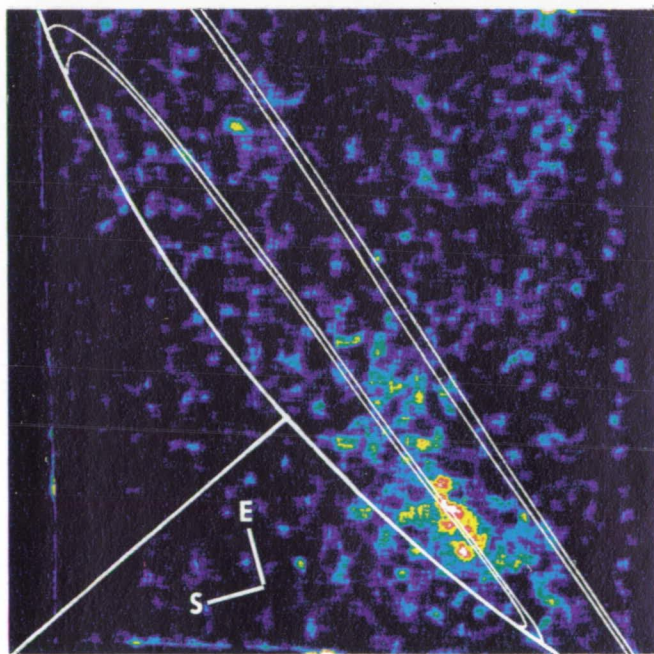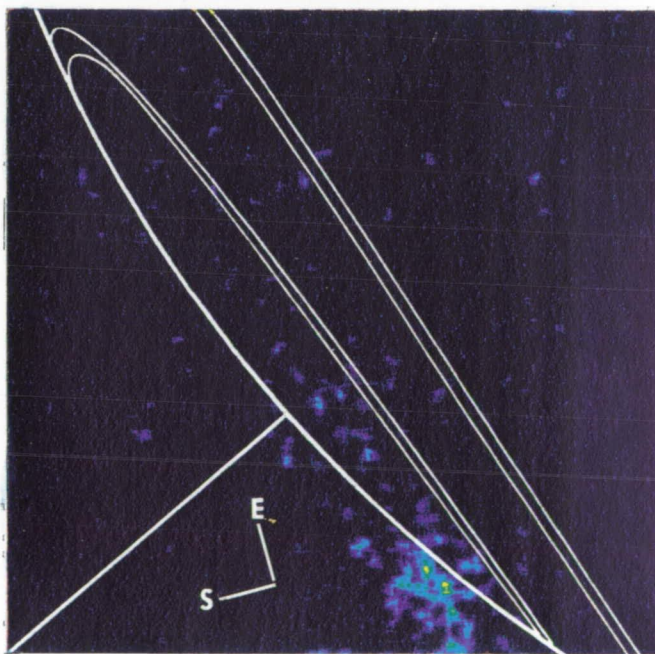
Figure 2b. Reduced HST FOC images of the south pole showing bright auroral features and shading that indicate Jovian magnetic coordinates for Io plasma torus auroral zone low latitude circle and magnetopause auoroal zone smaller inner circle.
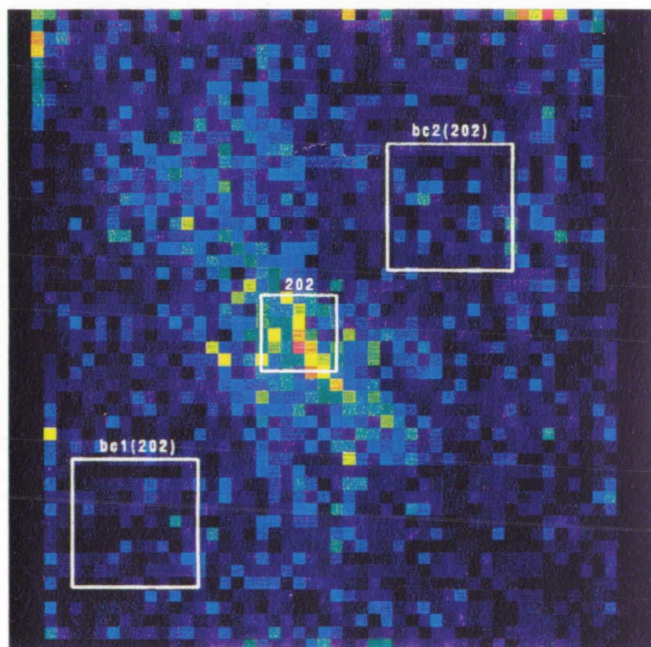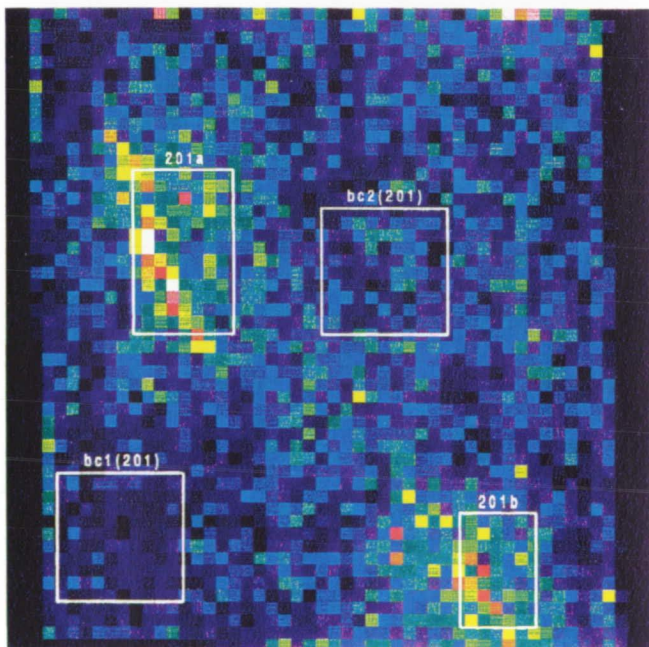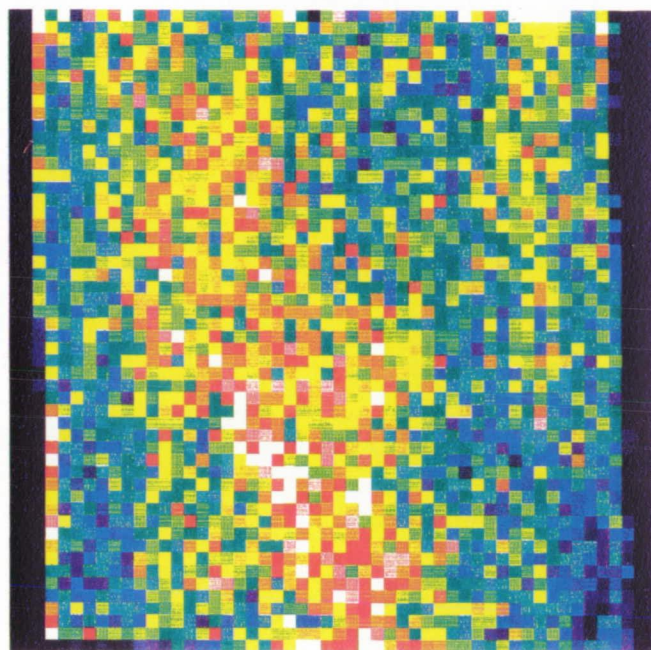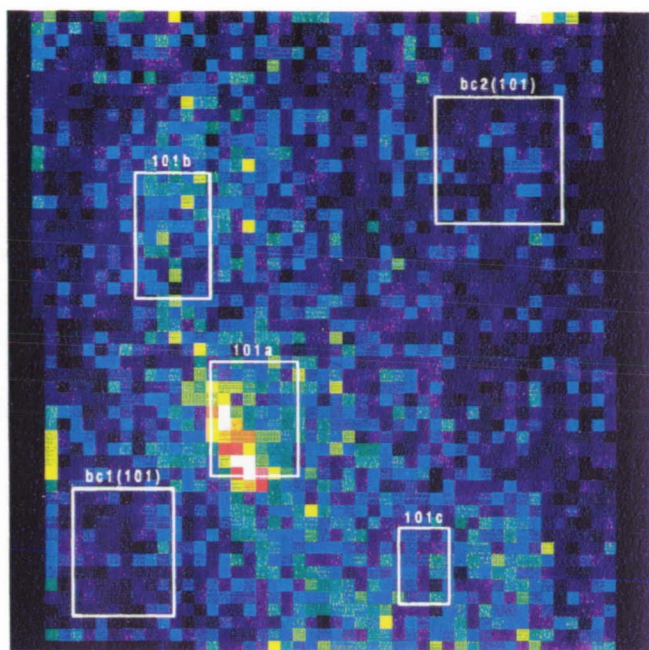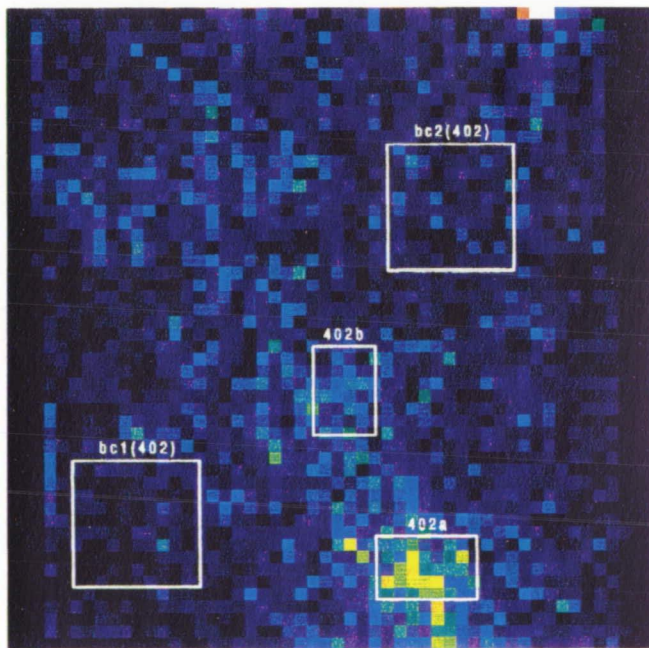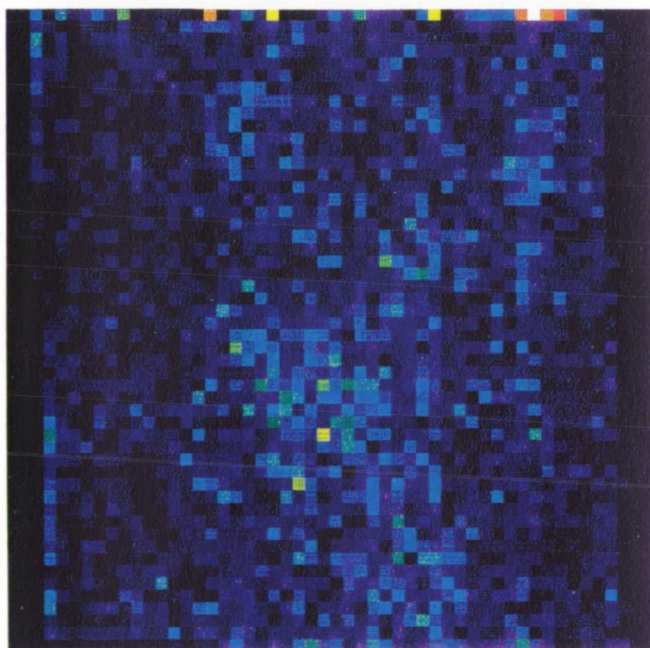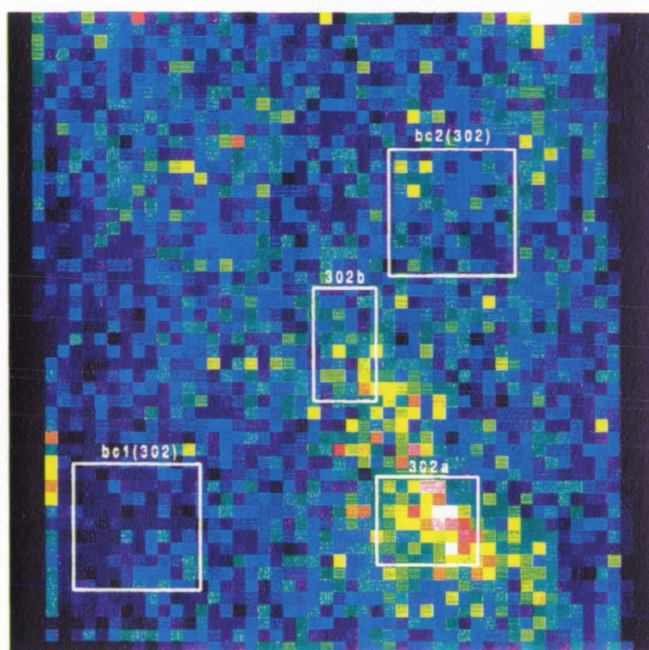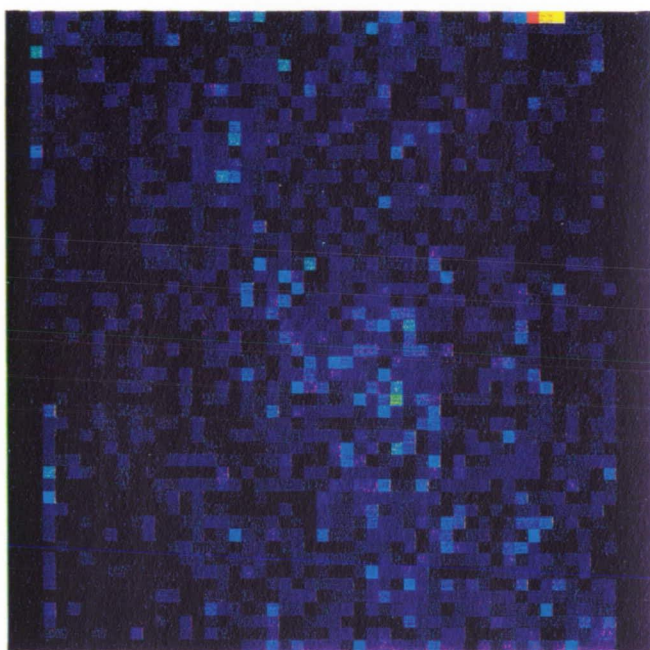
Figure 3a

Figure 3b

ROSAT PSPC PHOTON ENERGY SPECTRUM

—— BEST TWO LINE MODEL FIT
0.01 keV WIDTH AT 0.2 keV
0.7 keV WIDTH AT 0.9 kev
CHI SQUARE = 17

········ BEST BREMSSTRAHLUNG FIT
T = 0.47 keV
CHI SQUARE = 35

COUNTS

keV
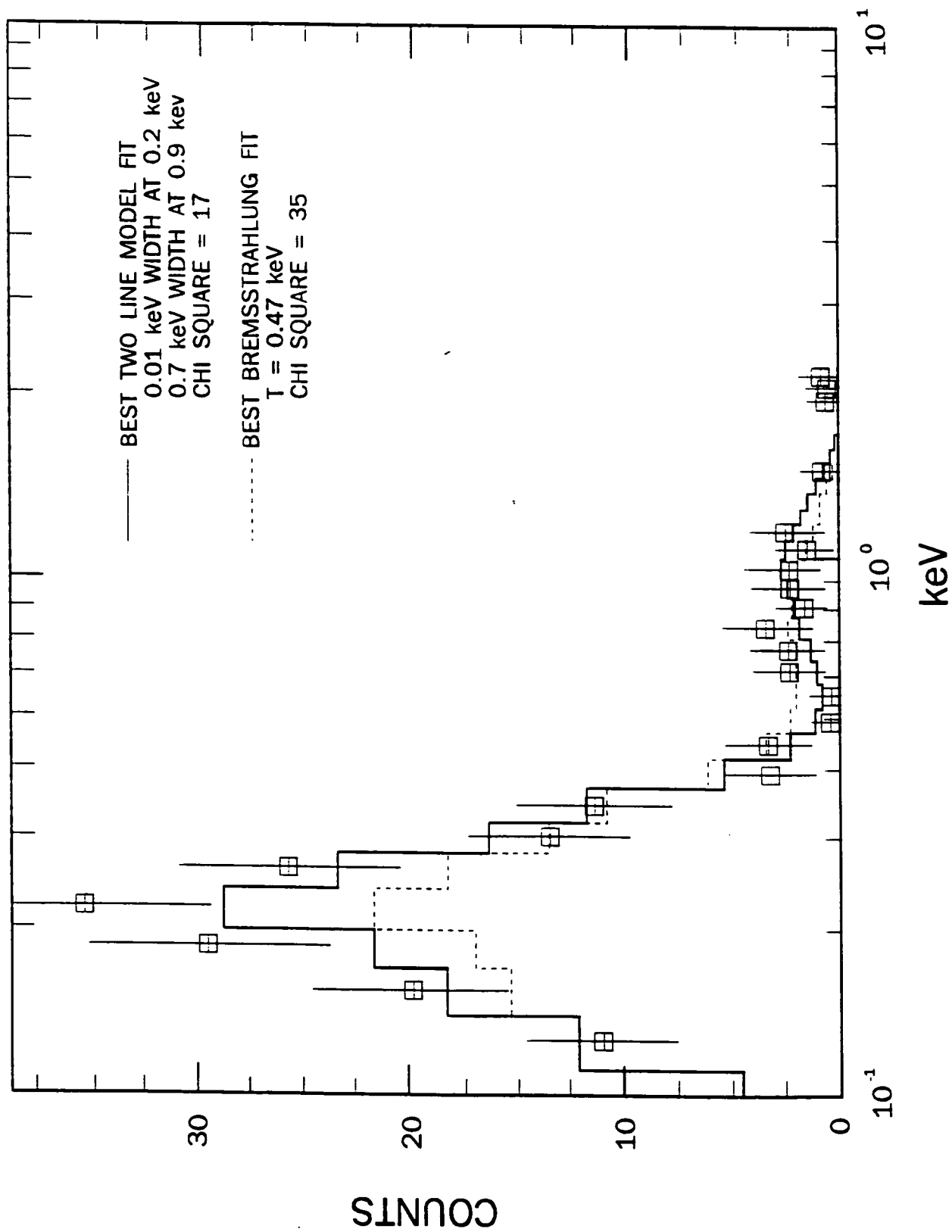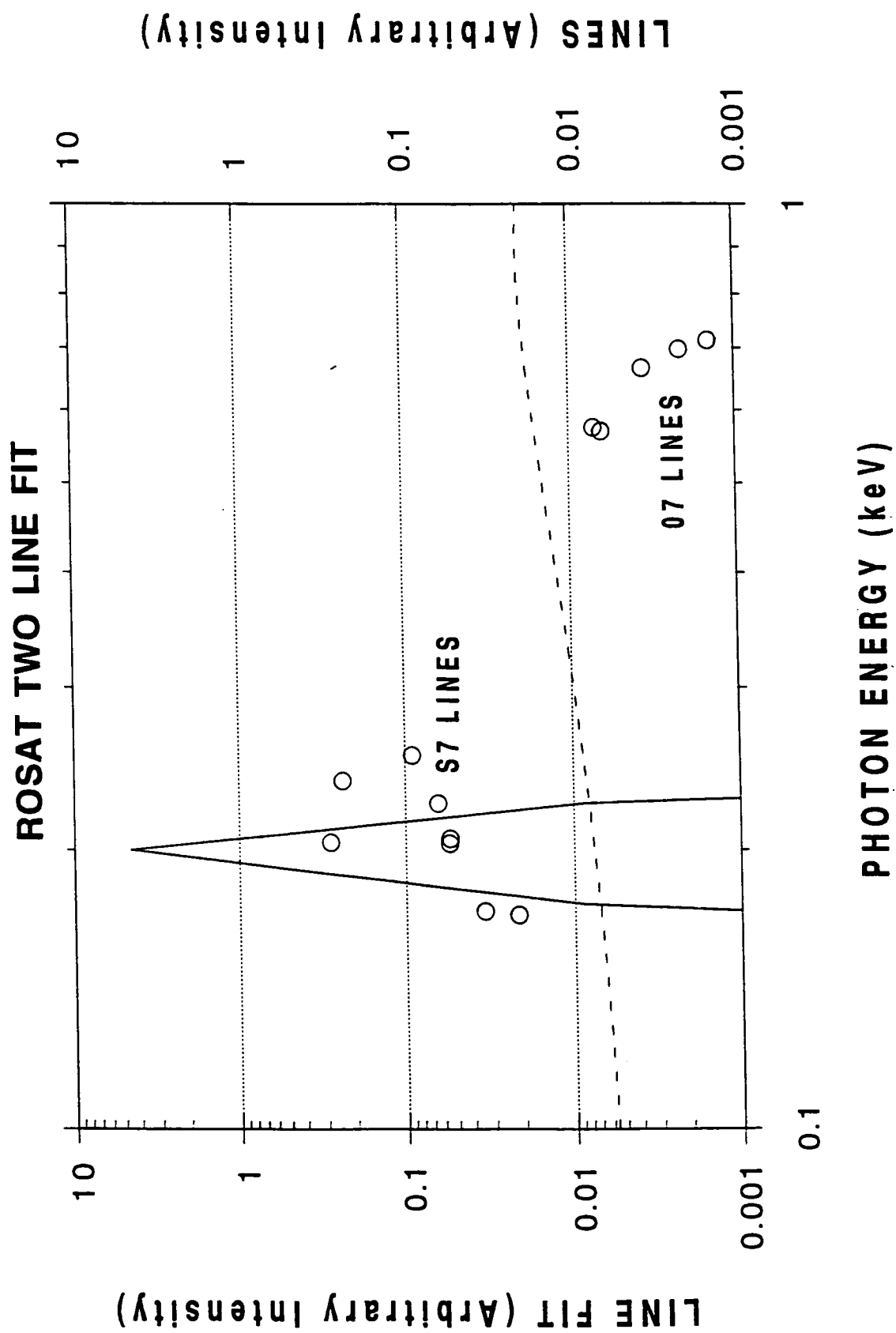
Figure 4

Figure 5

OXYGEN CHARGE STATE FRACTIONS

ENERGY (Log keV/amu)

EQUILIBRIUM FRACTION

Figure 6